

# Should anthropomorphic systems be “redundant”?

Ali Marjaninejad and Francisco J. Valero-Cuevas

## Abstract

We explore the conceptual design and implementation of muscle redundancy and kinematic redundancy for anthropomorphic robots from three perspectives: (i) The control of tendon-driven systems, (ii) How the number of muscles define functional capabilities, and (iii) How too few synergies can be detrimental to functional versatility.

Historically, roboticists prefer either rotational actuators located at each joint (i.e., rotational degree-of-freedom, DOF), or few linear actuators (i.e., two dedicated muscles per joint) for tendon-driven robots. In contrast, biological limbs have evolved to include too many muscles [1], which are thought to unnecessarily complicate their anatomy and control. The question, then, is why has evolution converged on these apparently under-determined (or redundant) solutions? If we really have extra muscles, then which muscle would you give up? By taking a formal mathematical approach to the control of tendons—which is the actual problem that confronts the nervous system—we have proposed a resolution to this apparent paradox by proposing that vertebrates may have, in fact, barely enough muscles to meet the numerous physical constraints for ecological functions (as opposed to simple laboratory tasks) [1, 2]. This approach can be called Feasibility Theory, which describes how the anatomy of the system, and the constraints defining the task define the set of feasible actions the system can produce. The role of the (neural or engineered) controller is then, to find ways to use the mechanical capabilities of the combined controller-plant system to the fullest [1].

Similarly, the effective mechanical design of a robotic limb, at a minimum, requires

---

Ali Marjaninejad

Department of Biomedical Engineering, University of Southern California, Los Angeles, CA, USA. e-mail: marjanin@usc.edu

Francisco J. Valero-Cuevas (To whom correspondence should be directed)

Departments of Biomedical Engineering, Electrical Engineering (Systems), Computer Science, and Mechanical & Aerospace Engineering, and Division of Biokinesiology & Physical Therapy, University of Southern California, Los Angeles, CA, USA. e-mail: valero@usc.edu

controllability (i.e., enough control degrees of freedom, or muscles) to produce arbitrary forces and movements (i.e., changes of state [3]). Force and movement capabilities have distinct governing equations and are, in fact, in competition with one another (e.g., a see-saw demonstrates, as per the Law of Conservation of Energy, how producing higher forces is associated with lower velocities and vice versa). Therefore, we explored the potential evolutionary pressures that may have shaped vertebrate limbs by evaluating how the number of muscles affects the competing demands to produce endpoint forces and velocities.

A related concept that cuts across biological and robotic systems is the idea that the kinematics and kinetics of a wide variety of actions exhibit a low-dimensional structure that can be approximated with a few principal components (sometimes called descriptive synergies [4, 5]). This has been taken to mean that a few degrees of freedom suffice to produce versatile behavior in the real world. However, the fine behavioral details that distinguish different actions are, by definition, not captured by the commonalities among them. Thus, versatility in the real world likely depends on recognizing and executing fine distinctions among actions; which implies that more degrees of freedom of control are critical for true functional versatility.

These three independent arguments support the perspective that creating anthropomorphic systems requires apparently redundant structures, because only then can they truly execute a wide variety of real-world tasks. In addition, we also present an open-access MATLAB toolbox that allows users from different backgrounds to explore these concepts in detail. We believe this new perspective will improve the conceptualization, understanding, and design of anthropomorphic systems.

## 1 Mechanical and neural foundations of Feasibility Theory

In this section, we provide fundamental concepts required to study neuromechanical systems, which will set fundamentals for the following sections of this chapter. We begin with limb kinematics, providing a common conceptual language to muscle mechanics. Next, we introduce motor control and feasible movements of tendon driven limbs to show how tendon-driven systems are in fact over-determined. Due to the inherent properties of biological muscles, the nervous system is likely not as redundant as when considering the force control problem in isolation. Moreover, we have described how different task constraints (i.e., the mechanical definition of the task) naturally limit feasible actions. Thus, each additional muscle adds an additional control DOF—and therefore the ability to meet more simultaneous functional constraints and produce a wider variety of tasks—which is the origin of versatility. Many of the materials and concepts of this section are summarized or first introduced in [1].

## 1.1 Limb kinematics and limb mechanics

We first start with limb kinematics, which characterize the motions and positions of rigid bodies, regardless of the forces which produce them. In this chapter, in order to simplify the governing equations, we consider limbs as rigid bodies. Subsequently, we introduce equations for limb mechanics which involve limb kinematics as well as the forces and torques that interact with the limb.

### 1.1.1 Limb kinematics

We first define a limb as a set of connected links and hinges. The endpoint of a multi-joint limb is defined by the homogeneous transformation matrix  $T_{base}^{endpoint}$ .  $T_{base}^{endpoint}$  can also be written as the multiplication of the DOF transformation matrices:

$$T_{base}^{endpoint} = T_0^N = T_0^1 T_1^2 \cdots T_{N-2}^{N-1} T_{N-1}^N \quad (1)$$

where each transformation matrix is defined as:

$$T_i^j = \begin{pmatrix} R_i^j & \mathbf{p}_{i,j} \\ 0 & 0 & 0 \\ 0 & 0 & 1 \end{pmatrix} \quad (2)$$

In the above equation,  $R_i^j$  represents the rotation matrix and  $\mathbf{p}_{i,j}$  represents the displacement for each DOF [1]. A schematic representation of the system for Eq. 1 is plotted in Fig. 1. Furthermore, the forward kinematic model (also known as the geometric model),  $G(\mathbf{q})$ , for a planar system (in two-dimensional space) is defined as follows (given that a rigid body on the plane has three degrees of freedom defining its location and orientation):

$$G(\mathbf{q}) = \begin{pmatrix} \text{displacement in the direction of } i_0 \\ \text{displacement in the direction of } j_0 \\ \text{rotation about the } k_0 \text{ axis} \end{pmatrix} = \begin{pmatrix} x \\ y \\ \alpha \end{pmatrix} \quad (3)$$

For non-planar limbs, displacement in the direction of  $k_0$ , rotation about the  $i_0$ , and rotation about the  $j_0$ , will also need to be included in  $G(\mathbf{q})$  [1]. The endpoint velocities are obtained by differentiating  $G(\mathbf{q})$  with respect to time:

$$\dot{G}(\mathbf{q}) = \frac{dG(\mathbf{q})}{dt} = \frac{\partial G(\mathbf{q})}{\partial \mathbf{q}} \frac{d\mathbf{q}}{dt} = \frac{\partial G(\mathbf{q})}{\partial \mathbf{q}} \dot{\mathbf{q}} = \begin{pmatrix} \dot{x} \\ \dot{y} \\ \dot{\alpha} \end{pmatrix} \quad (4)$$

We call  $\frac{\partial G(\mathbf{q})}{\partial \mathbf{q}}$  as the Jacobian matrix. For a limb with N degrees of freedom, it is defined as:

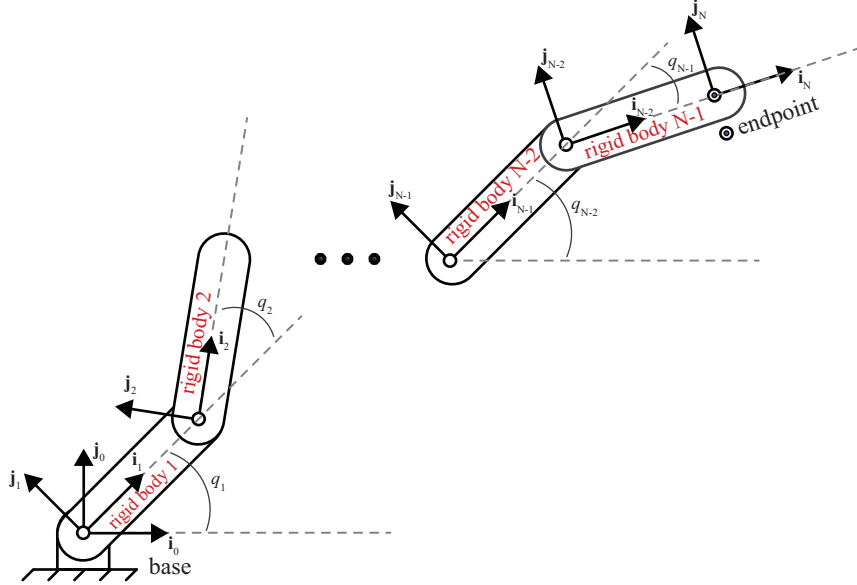


**Fig. 1** A schematic representation of a simple multi-link system. (Reproduced, with permission, from [1])

$$\frac{\partial G(\mathbf{q})}{\partial \mathbf{q}} = J(\mathbf{q}) = \begin{bmatrix} \frac{\partial G_x(\mathbf{q})}{\partial q_1} & \frac{\partial G_x(\mathbf{q})}{\partial q_2} & \dots & \frac{\partial G_x(\mathbf{q})}{\partial q_N} \\ \frac{\partial G_y(\mathbf{q})}{\partial q_1} & \frac{\partial G_y(\mathbf{q})}{\partial q_2} & \dots & \frac{\partial G_y(\mathbf{q})}{\partial q_N} \\ \frac{\partial G_\alpha(\mathbf{q})}{\partial q_1} & \frac{\partial G_\alpha(\mathbf{q})}{\partial q_2} & \dots & \frac{\partial G_\alpha(\mathbf{q})}{\partial q_N} \end{bmatrix} \quad (5)$$

### 1.1.2 Limb mechanics

As mentioned earlier, limb mechanics involve limb kinematics as well as the forces and torques the limb can produce. In this section, we will explain how to relate joint torques to endpoint forces using limb kinematics. Lets begin by defining the internal and external work for the two DOF systems shown on Fig. 2 as:

$$External\ work = \mathbf{f} \cdot \Delta \mathbf{x} \quad (6)$$

$$Internal\ work = \boldsymbol{\tau} \cdot \Delta \mathbf{q} \quad (7)$$

where  $\mathbf{f}$  and  $\Delta \mathbf{x}$  are scalar values representing endpoint force and endpoint velocity, while  $\boldsymbol{\tau}$  and  $\Delta \mathbf{q}$  are torque and joint angle rotation vectors. Please note that, depending on the kinematic DOFs of the system, the endpoint can also produce a torque ( $\tau_{endpoint}$ ), whose external work would be it times the rotation of the endpoint. For the sake of simplicity, here we present the derivation only considering

endpoint forces. Following with Eq. 7 and Eq 8, from the conservation of energy law, we have:

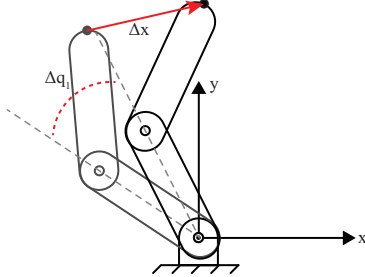


**Fig. 2** An illustration of the geometric relationship between the endpoint displacement ( $\Delta\mathbf{x}$ ) and the rotation of the first joint ( $\Delta q_1$  in a 2-DOF limb). (Reproduced, with permission, from [1])

$$\mathbf{f} \cdot \Delta\mathbf{x} = \boldsymbol{\tau} \cdot \Delta\mathbf{q} \quad (8)$$

Changing the dot product in Eq. 8 to its equivalent inner product while substituting  $\Delta$  for both  $\mathbf{x}$  and  $\mathbf{q}$  with derivatives, we have:

$$\mathbf{f}^T \dot{\mathbf{x}} = \boldsymbol{\tau}^T \dot{\mathbf{q}} \quad (9)$$

Using Eqs. 4 and 5, we rewrite Eq. 8 as:

$$\mathbf{f}^T J(\mathbf{q}) \dot{\mathbf{q}} = \boldsymbol{\tau}^T \dot{\mathbf{q}} \quad (10)$$

Eliminating  $\dot{\mathbf{q}}$  from both sides of the equation leads to Eqs. 11 and 12, which define the relationship between the joint torques and endpoint forces.

$$\mathbf{f}^T J(\mathbf{q}) = \boldsymbol{\tau}^T \quad (11)$$

$$\mathbf{f}^T = J(\mathbf{q})^{-1} \boldsymbol{\tau}^T \quad (12)$$

Extensions of this concept for 3-dimensional space with detailed examples are provided in [1].

### 1.1.3 Tendon-driven limb mechanics

Most robotic limbs are driven by either rotational or linear actuators that drive each kinematic DOF [1]. In the robotics literature, the so-called torque-driven formulation assumes symmetric actuators. That is, equal torque capabilities in both clockwise and counterclockwise directions.

In the so-called tendon-driven systems, actuators are connected to the limbs using strings, cables, or tendons. It is clear that these actuators can only pull (and not push) on the tendons, thus they can only drive the DOF in one direction. Therefore, each DOF requires, on average, more than one actuator and symmetry of actuation is not guaranteed. In addition, tendon-driven systems are flexible because the routing of their tendon can allow one actuator to drive more than one DOF—and therefore impose correlations in actuation across DOFs [6, 7]. Moreover, the moment arms (i.e., minimal perpendicular distance between the tendon path and the center of rotation of the DOF) can be arbitrarily set within and across tendons and DOFs.

This flexibility of actuation that can be built into the morphology of the design, compared to torque-driven systems, introduces unique flexibility and challenges to their construction and control. To some, this means that tendon-driven systems are unnecessarily difficult to build and control. However, we and others also argue that they have much to offer [7–13]. Using tendons to apply torque to the DOFs, as opposed to having actuators directly apply torque, makes tendon-driven systems capable of remote actuation. This means that the designer can place the actuator far from the joint itself. Although making the system harder to control, flexible tendon routing can provide much more versatility and preferentially larger feasible endpoint forces and velocities in directions of interest.

### 1.1.4 Tendon actuation

To explore how tendons create torque in tendon driven systems, see Fig 3. This simplified model illustrates a planar, one-joint limb using one muscle. The torque at the joint of this model is equivalent to the cross-product of the force and moment arm  $r$ :

$$\tau = r \times f_m = \|r\| \|f_m\| \sin(\alpha) \quad (13)$$

where  $\times$  represents the cross-product,  $f_m$  represents the muscle force, and  $\alpha$  represents the angle between the force and the moment arm.

As mentioned earlier, in tendon-driven systems, one actuator can exert torque in multiple DOFs. Here, we are going to study an example of such while introducing the moment arm matrix. We begin by illustrating the relationship between the torque vector (here, a vector of length two, representing the two DOFs) and muscle force vector for the two-joint planar limb shown in Fig. 4:

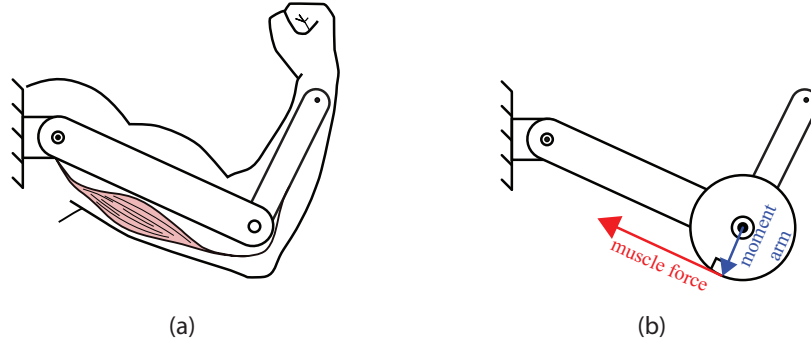


**Fig. 3** Schematic representation of a planar, two joint limb with only one muscle (a) and its equivalent simplified model (b).

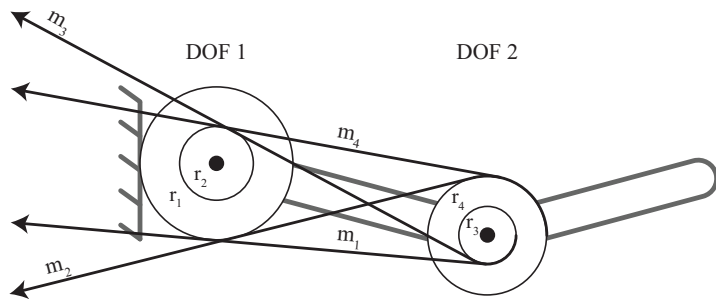


**Fig. 4** A sample two-joint limb with four muscles. (Reproduced, with permission, from [1])

$$\begin{pmatrix} \tau_1 \\ \tau_2 \\ \vdots \\ \tau_M \end{pmatrix}_{M \times 1} = R(\mathbf{q})_{M \times N} \begin{pmatrix} f_1 \\ f_2 \\ \vdots \\ f_N \end{pmatrix}_{N \times 1} \quad (14)$$

where  $R(\mathbf{q})$  represents the moment arm matrix, which maps the muscle forces to the joint torques. In example illustrated in Fig. 4, the moment arm matrix  $R(\mathbf{q})$  is defined as:

$$R(\mathbf{q}) = \begin{bmatrix} -r_1 & -r_1 & r_2 & r_2 \\ -r_3 & r_4 & -r_3 & r_4 \end{bmatrix} \quad (15)$$

By convention, each entry in the moment arm matrix on the  $i^{th}$  row and  $j^{th}$  column will be the coefficient which transforms the force induced by the  $i^{th}$  muscle to the torque exerted at the  $j^{th}$  joint (as seen in Eq. 9). The positive value of an element in this matrix means that counterclockwise (positive) torque will be applied when

tension is applied to the tendon through muscle contraction (applying concentric force).

In order to relate muscle excursions to joint movements in the model shown above, we produce a set of equations. Again, by convention, we consider counter-clockwise rotations as positive rotations. Following the conventions we have mentioned so far, a positive joint rotation with a positive moment arm induces a shortening in the length of its muscle and tendons and vice versa. Therefore, the set of equations relating joint angles and muscle excursions for the example provided in Fig. 4 will be as follows:

$$\begin{pmatrix} \partial S_1 \\ \partial S_2 \\ \partial S_3 \\ \partial S_4 \end{pmatrix}_{4 \times 1} = \begin{bmatrix} r_1 & r_3 \\ r_1 & r_4 \\ -r_2 & r_3 \\ -r_2 & r_4 \end{bmatrix}_{4 \times 2} \begin{pmatrix} \partial q_1 \\ \partial q_2 \end{pmatrix}_{2 \times 1} \quad (16)$$

Using Eq. 9, we can rewrite Eq. 10 in the general case with M joints and N muscles as:

$$\begin{pmatrix} \partial S_1 \\ \partial S_2 \\ \vdots \\ \partial S_N \end{pmatrix}_{N \times 1} = (-R_{M \times N})^T \begin{pmatrix} \partial q_1 \\ \partial q_2 \\ \vdots \\ \partial q_N \end{pmatrix}_{M \times 1} \quad (17)$$

Taking a closer look at Eq. 14 and Eq. 17, we see a very important distinction. Equation 14 is under-determined, meaning that there is more than one solution in the force space to achieve the desired set of torques. This is one of the main reasons that neuromuscular systems are thought to be redundant. However, looking at Eq. 17, we notice that this equation is over-determined, meaning there is, at maximum, only one set of values for the joint angles fulfilling this set of equations [1, 6, 14]. In other words, you cannot contract and shorten a specific muscle without having changes in the lengths of other muscles connecting to or passing through the same joint. It illustrates that our nervous system must consider a complex variety of constraints when pulling a tendon. Failure in fulfilling the requirements of this complex control problem, especially failure in relaxing muscles that are being lengthened as a result of joint rotations, might disrupt movement or injure muscles or tendons [6, 15]. Note that this over-determined case only arises when treating limbs as tendon-driven systems. This is one of the important, yet mostly overlooked aspects of robotics today.

## 1.2 Motor control of tendon driven limbs and Feasibility Theory

In this section, we describe the tendon-driven system that the nervous system faces. First, we present a conceptual framework where one can think of neural commands as being a high-dimensional activation vector that is mapped into lower-dimensional “spaces”, that capture its transformation into endpoint forces. Next, we describe Feasibility Theory, which defines how different constraints can limit the feasible activations in different spaces (activation, muscle force, torque, and end-point force spaces). If we are looking for a versatile system to deal with day to day activities, then a larger number of DOFs are required as constraints are added.

### 1.2.1 Motor control of tendon driven limbs

Although the nervous system activates muscles through the recruitment of motor neurons and modulation of their firing rates, we can, without loss of generality, simplify the problem by assigning a value between 0 and 1 to the activation level of each muscle, where 0 represents complete inactivation and 1 represents maximal activation. The activation vector  $\alpha$  is described as Eq. 18 for an  $N$  muscle system:

$$\alpha = \begin{pmatrix} \alpha_1 \\ \alpha_2 \\ \vdots \\ \alpha_N \end{pmatrix}, \quad 0 \leq \alpha_i \leq 1 \text{ for } i = 1, \dots, N \quad (18)$$

where  $\alpha_i$  is the activation value for the  $i^{th}$  muscle. Now the set of the generated muscle forces at a particular moment and at a particular activation level can be defined as:

$$\mathbf{f}_m = F_0(\mathbf{l}_m, \mathbf{v}_m)\alpha \quad (19)$$

where  $F_0$  is the diagonal matrix. Each element on the main diagonal of this matrix will represent the maximum force that the corresponding muscle can exert. These diagonal values depend on many factors such as muscle architecture, pennation angle, physiological cross-sectional area, as well as the fiber length ( $l_m$ ) and velocity ( $v_m$ ) of the muscle at every time point. Now, we rewrite Eq. 14 by substituting the force vector from Eq. 19, which leads to the following equation:

$$\tau_{M \times 1} = R(\mathbf{q}_{M \times N}) F_0(\mathbf{l}_m, \mathbf{v}_m)_{N \times N} \alpha_{N \times 1} \quad (20)$$

Eq. 20 shows that the control of joint torques in tendon-driven limbs is an under-determined set of equations. However, adding a cost function which needs to be

minimized (e.g. the total sum of the activation values), will force this set of equations to have fewer possible solutions (or even just one).

Considering the fact that maximum muscle force values (the diagonal values on the  $F_0$  matrix) are also functions of muscle length and velocity, we see that discovering the activation values which result in a desired set of joint torques (Eq. 20) is difficult. In fact, it will apply constraints to the solutions that the nervous system can produce. We discuss the effects of these constraints in greater detail in the following sub-section, which explains how our nervous system faces a much more complex control problem than initially hypothesized in the literature [16].

Reconsidering the set of tendon excursions, we can rewrite Eq. 17 in terms of the muscle length vector,  $\mathbf{l}_m$ , and muscle velocity vector,  $\mathbf{v}_m$  (Eq. 21 and Eq. 22).

$$(\delta \mathbf{l}_m)_{N \times 1} = (-R_{M \times N})^T \delta \mathbf{q}_{M \times 1} \quad (21)$$

$$(\mathbf{v}_m)_{N \times 1} = (-R_{M \times N})^T \dot{\mathbf{q}}_{M \times 1} \quad (22)$$

These last two sets of equations illustrate how control of tendon excursions is an over-determined problem (i.e. there is, at most, only one set of solutions for it). Therefore, our nervous system faces a biomechanical limitation [1].

### 1.2.2 Feasibility Theory: Defining feasible sets of actions in tendon-driven limbs

In this section, we first explore how a neural activation vector is mapped into the torque space and the effect of different biomechanical parameters on this mapping. Next, we demonstrate how functional constraints can limit the feasible action spaces, therefore making it harder for the controller to find a solution within these spaces [16].

Lets assume we have three muscles, representing their activation values as  $a_1$  to  $a_3$ . A rectangular cuboid can be used as a visual representation of these activations. This cuboid is shown in Fig. 5a. The corresponding muscle force vector is determined by Eq. 19 and represented in Fig. 5b. Now, lets say we have a two DOF joint. This assumption means that our feasible muscle force set (Fig. 5b), which is a three-dimensional cuboid, will be mapped into the two-dimensional feasible torque space. The amount of torque generated at each joint is determined by Eq. 20. The feasible torque set for this example is shown in Fig. 5c. We utilize the appropriate Jacobean matrix, mapping this feasible torque set to the feasible end-point force set using Eq. 12. The feasible force set for this example is shown in Fig. 5d. Looking at the different parts of Fig. 5 we can see the contributions of having extra muscles in each of these feasible action spaces.

For the example in Fig. 5, lets now assume that there is a functional constraint. This may include a certain constraint on the magnitude of the force in one axis in the end-point force space, or a certain torque in the torque space, etc. Since the torque or the end-point force spaces are two-dimensional in this example, these

constraints can only be points or lines in these spaces. However, when we track them back into the muscle activation space (or muscle force space), they can be points, lines, or planes (or hyper-planes in more than three dimensional spaces) since all the transformations are linear. Say we have defined a constraint whose representation in the muscle activation space is a plane (i.e. the constraint plane). The new feasible activation set now is the intersection of the feasible activation set, without any constraints, with this constraint plane. This new feasible activation set is shown in Fig. 6a. If more constraints are added, the feasible muscle activation set will lose even more dimensions and might become a line, a point, or an empty set (Fig. 6b-d). This shows that while creating a specific amount of end-point force or torque in a joint can be an under-determined problem, functional constraints and feasible action spaces (as well as the mapping functions between these spaces) can limit the abilities of our neuromechanical system to a great extent [1, 16]. Therefore, the control problem which the nervous system faces is a very complicated one.

This suggests that having extra muscles is not redundant, but is a necessary requirement for versatility. Extra sets of muscles will increase the DOF of the system while enabling the nervous system to find solutions for different sets of problems we face daily.

## **2 An evolutionary fitness approach to the relationship between the number of muscles and versatility**

Throughout the years, many have wondered why the anatomy of vertebrates has evolved to include a seemingly redundant number of muscles. Here we show how extra muscles can enhance mechanical versatility using an evolutionary approach while clarifying why muscle redundancy is not a comprehensive belief. We begin our study by observing how our biomechanical tendon-driven model performs a set of specified kinetic tasks while changing the number of muscles. We study the optimal number of muscles with three main fitness functions. Namely, the Effectiveness, Agility, and Phenotypical cost. During all tasks, the goal was to apply maximum force in a specific direction. We found the optimal activation values as a function of task restraints using a linear optimization algorithm.

### **2.1 Background**

Muscle redundancy has been discussed extensively ever since the earliest neuromuscular studies. Evolution from the earliest ape species, *Nakalipithecus nakayamai*, to modern *Homo Sapiens*, exemplifies the growth and development of muscles, enabling our species to perform multiple tasks. There are certain questions that resurface each time someone tries to explore this field. Why do we have so many muscles despite the limited degrees of freedom in our limbs or fingers? Why do we have that

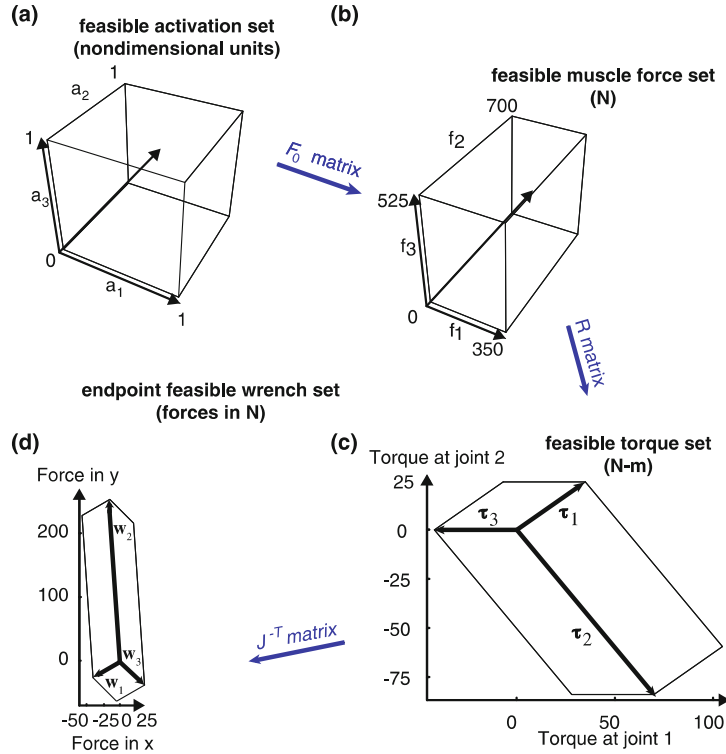


**Fig. 5** The representation of the feasible actions in different spaces for the toy example discussed in the text. (a) the feasible set of activations. (b) the feasible set of muscle forces. (c) the feasible set of joint torques. (d) the feasible set of end-point forces. (Reprinted, with permission, from [1])

specific number of muscles? What are the costs and benefits of having this set of muscles?

In this section, we explore answers to these questions with an evolutionary fitness approach. We study how extra sets of muscles affect Effectiveness, Agility, and Phenotypical cost (we will describe each later in this section). In addition to this, we explore how decreasing the number of muscles affects performance in different tasks. In this study, we have used a 2-DOF arm model with three different muscle sets.

## 2.2 Method

We first explain our model and assumptions. Next, we describe the simulated tasks used in this study. Finally, we introduce our fitness functions for each of the elements

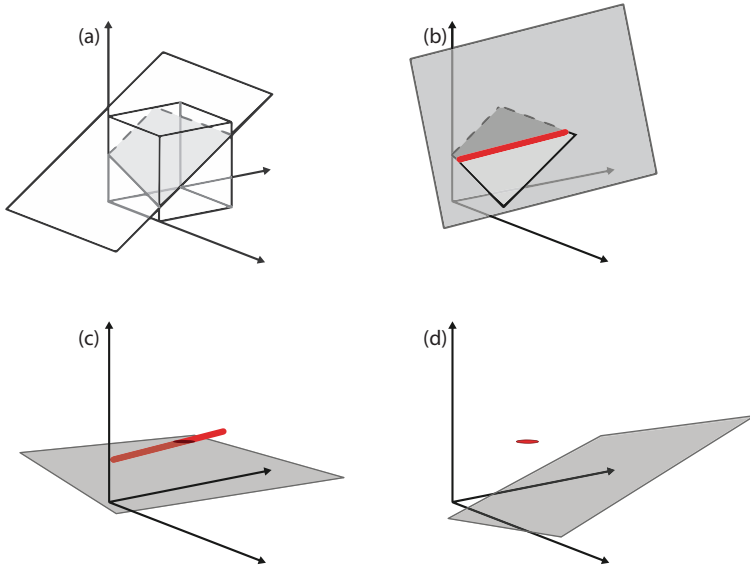


**Fig. 6** The effects of adding functional constraints on the feasible actions spaces. More and more constraints are applied as we move from (a) to (d). (Reproduced, with permission, from [1])

mentioned earlier as well as the Overall Fitness, which is the weighted linear combination of all the individual fitness functions. Note that we use the term “fitness” in the general sense where it is not necessarily tied to a single specific cost function. Rather, fitness in the biological sense indicates the ability to meet current multi-dimensional requirements and perform well in a given environment. For the sake of simplicity, we define fitness as the ability to meet a compound cost function—but other cost functions may also be suitable depending on the functional goals at hand.

### 2.2.1 Model

We begin with a simplified model of the human arm with a two DOF planar structure. One can also generalize this model to other body parts with similar structure e.g. fingers. We select four postures based on common tasks performed by the arm, as shown in Fig. 7. Each posture was held static while force was maximized in four directions: upward, downward, frontward, and backward.

Three muscle sets were designed to compare the effects of varying the number of muscles. These muscle sets, shown in Fig. 8, were designed with the intent of recreating a model with a realistic set of arm muscles (although this model is constrained to two-dimensional space) as well as models with fewer or more muscles than a real arm. Across muscle sets, the number of muscles was decreased while keeping the same original routing configuration of the previous muscle set. This was done

to compare the effects of decreasing or increasing the number of muscles only. The moment arms were estimated with reference to [1].

We selected 3, 7, and 14 as the number of muscles which are the minimum number of muscles for a 2-DOF system, the real number of muscles in a human arm and two times of the number of muscles in a human arm, respectively. In the Monte Carlo analysis, the moment arm values were varied by  $\pm 20\%$  over 100 simulations to test the sensitivity of the results to these values.

### Model assumptions

In this study, all muscle lengths and maximum muscle forces were assumed to be equal enabling us to address only a specific set of questions. We study how the number of muscles affects a specific set of outputs in the absence of other variables. Also, muscle forces were assumed to be independent from muscle lengths or muscle velocities.

#### 2.2.2 Cost formulation

Here we describe the performance metrics studied. First, we define the Average Energy as the summed square of muscle activation values, divided by the number of muscles. Although muscle activation is a neural action, it will be proportional to physical muscle activity (and therefore requires energy) since we assumed that all muscles have equal maximum force values. Average Energy shows how hard muscles pull on average to perform the task. The Average Energy will be as defined in the quadratic Eq. 23.

$$\text{Average Energy} = \frac{1}{N} \sum_{i=1}^N \alpha_i^2 \quad (23)$$

where  $\alpha_i$  is the activation of the  $i^{th}$  muscle (between 0 and 1) and  $N$  is the number of muscles [17, 18].

Although Average Energy shows the total amount of energy used to perform a task, it is not the best way to calculate Effectiveness since the maximum force output of a task is also very important. Therefore, we define Effectiveness as the maximum output force divided by the Average Energy. Note that Effectiveness is distinct from efficiency as we are using it to reflect overall ability after normalizing for energy consumption. Phenotypical cost (see below) already considers metabolism.

$$\text{Effectiveness} = \frac{\text{maximal force}}{\text{Average Energy}} \quad (24)$$

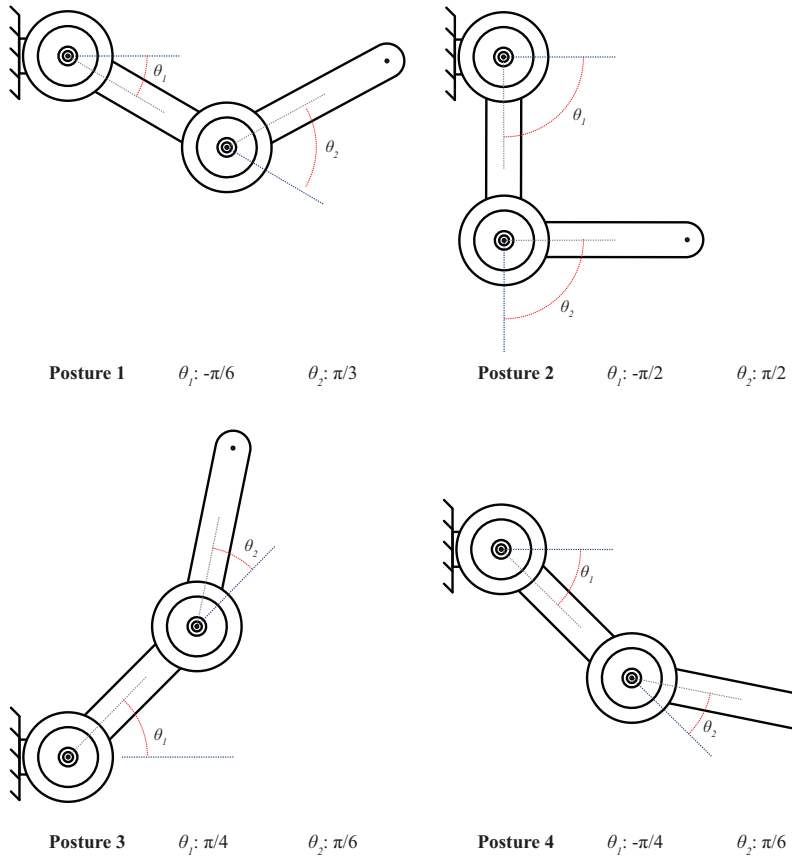


**Fig. 7** Four different postures used for simulations. These postures were inspired by day to day activities.

We know that there is a limit on how fast a muscle can contract (the maximum speed for muscle excursion). We define “Agility” for each joint as the maximum rate of change in the joint (regardless of the direction), assuming that the muscle excursions for all muscles have the same upper limit. This is similar to the concept of manipulability, which considers the transformation of joint angular velocities into endpoint velocities as per the Jacobian of the limb [19]. Therefore, Agility for each joint is defined as:

$$\text{Agility} = \frac{dq}{ds} = \max_{ij}(\text{abs}(\frac{1}{r_{ij}^T})) \quad (25)$$

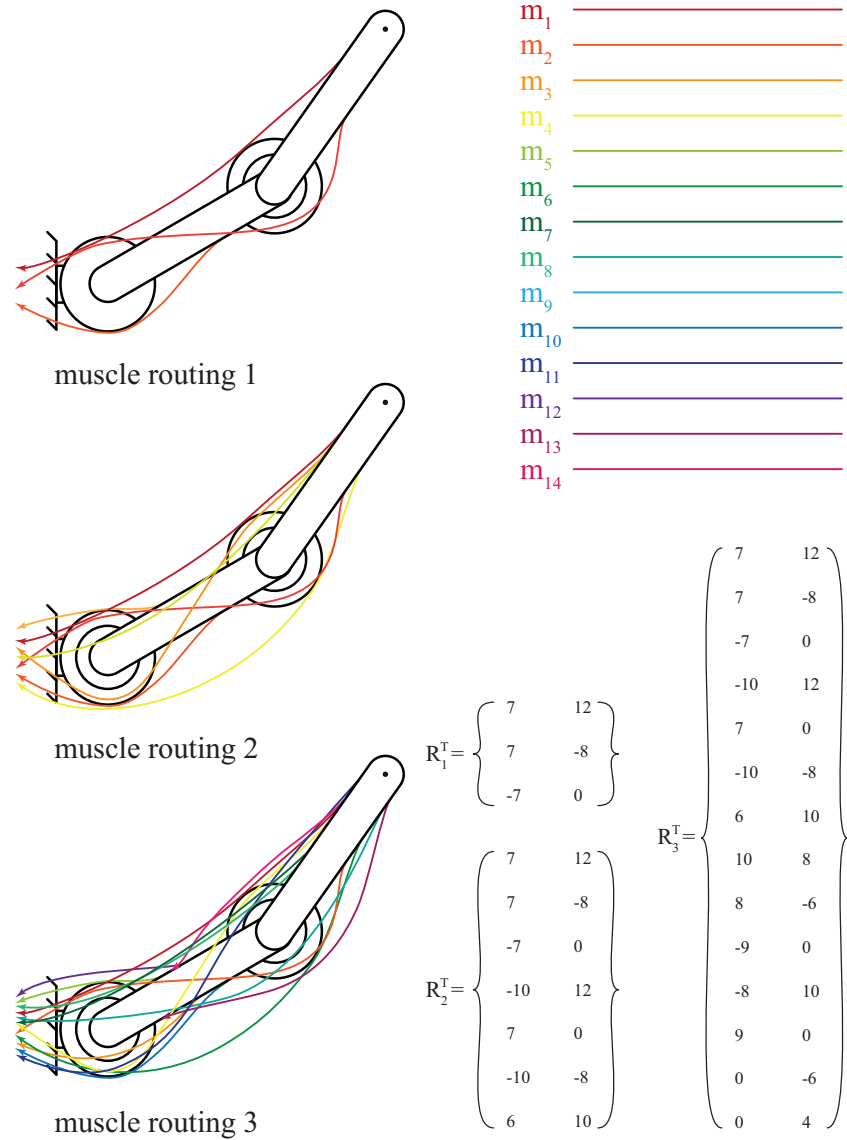


**Fig. 8** Muscle routings and moment arm matrices used in the simulations.

where  $i$  is the muscle index,  $r_i$  is the corresponding moment arm value,  $\max$  stands for maximum, and  $\text{abs}$  stands for absolute value. Please note that to maximize the  $\frac{dq}{ds}$ ,  $r_{ij}^T$  cannot be equal to zero, since this would mean that the muscle is not connected to the intended joint.

Lastly, the “Phenotypical” cost is related to the number of muscles due to the nature of muscle packaging [20]. In particular, the Phenotypical cost can consider both the cross-sectional area and volume of muscles and muscle groups. Therefore, we explored this value using the square and the cube of the number of muscles (Overall Fitness A and Overall Fitness B, respectively). The quadratic version preferentially considers metabolic and phenotypical costs associated with muscle stress and physiological cross-sectional area [21]; whereas the cubic version attempts to further penalize the complexity of vascularizing, repairing, maintaining, packaging and controlling more muscles [20].

To compute the fitness of alternative embodiments for a multi-muscle limb, we compute Overall Fitness as shown below. It is the weighted sum of the above-mentioned elements:

$$\text{Overall Fitness} = w_1 \times \text{Effectiveness}_N + w_2 \left( \frac{\text{Agility}_{N,1} + \text{Agility}_{N,2}}{2} \right) - w_3 \times \text{Phenotypical cost} \quad (26)$$

where  $\text{Effectiveness}_N$  and  $\text{Phenotypical cost}_N$ , are the normalized (between 0 to 1) Effectiveness and Phenotypical Cost, respectively.  $\text{Agility}_{N,k}$  is the normalized Agility in the  $k^{th}$  joint while  $w_1$ ,  $w_2$ , and  $w_3$  are weights for  $\text{Effectiveness}_N$ , average  $\text{Agility}_{N,k}$  (averaged over  $k$ ) and the  $\text{Phenotypical Cost}_N$  respectively.

We used linear programming [22] to find the solutions in the activation space for the constrained problem of maximizing the force in only the specified direction in each task.

### 2.3 Results

Figures 9 and 10 respectively demonstrate Average Energy and Effectiveness as a function of number of muscles for each posture. In addition, Agility was plotted as a function of number of muscles for each joint (Fig. 11). We then performed Monte Carlo analysis to determine the sensitivity of the results to the assumed values for the moment arm matrix. The results follow the same pattern regardless of the variation in values for the moment arm matrix, demonstrating that this analysis is generalizable to a large variation in moment arm values.

Our results show that increasing the number of muscles increases Effectiveness and Agility. However, it is clear that more muscles also have more Phenotypical cost. This is why we believe that there is a “sweet spot” for an optimal number of muscles, based on how much weight each of these goals have in an anthropomorphic system. These weights are set during evolution to find the optimal number of muscles to be as versatile as possible, while maintaining a reasonable Phenotypical cost. That is where the Overall Fitness, introduced in the methods section (Eq. 26), will be useful. The Overall Fitness plays a pivotal role by combining the weighted effect of each

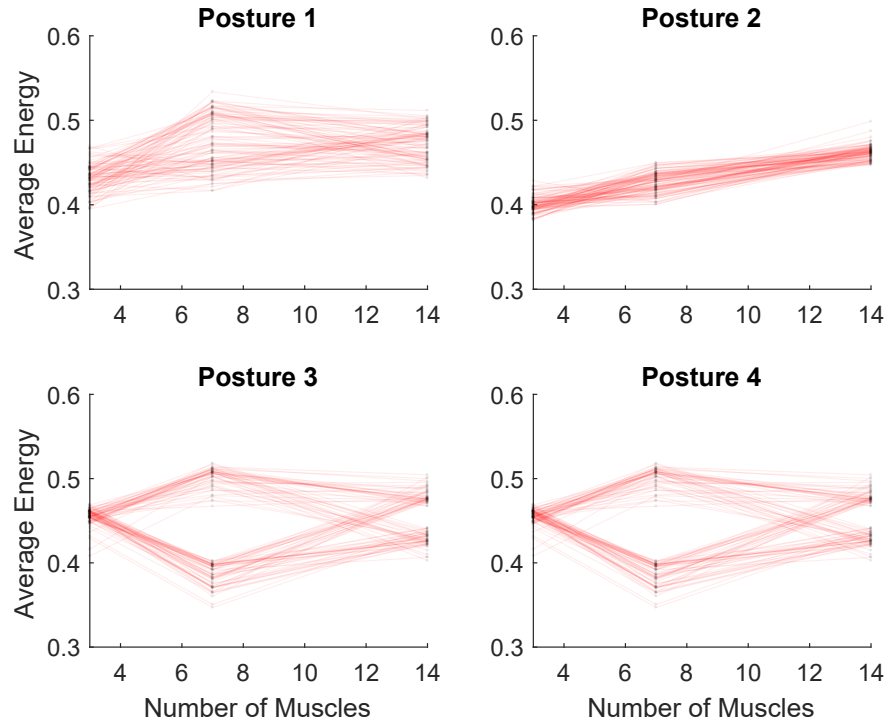


**Fig. 9** Average Energy plots (Monte Carlo analysis).

element and providing a single measure that needs to be optimized. Again, while adding extra muscles will increase Effectiveness (Fig. 10) and Agility (Fig. 11), it will also increase the Phenotypical cost. Therefore, for each system, the number of muscles for which this Overall Fitness is minimized is the optimal muscle number for that system.

By changing the weights in the Overall Fitness function, we can easily find the set of weights where 7 muscles (the real number of muscles in a human arm) are the optimal choice. As described before, these weights can be interpreted as the relative importance of each goal (Effectiveness, Agility, and low Phenotypical cost) to vertebrates, from an evolutionary point of view. By setting  $w_1$ ,  $w_2$ , and  $w_3$  to 4, 1, and 4 respectively, we have Fig. 12, which shows that the optimal number of muscles is 7.

Please note that there are many combinations of weights that can lead to a specific number of muscles. Similarly, any choice of cost function in the literature can be a matter of choice and preference [23]. We chose three fitness functions (Effectiveness, Agility and Phenotypical cost) to reflect the multi-dimensional nature of functional fitness. This, in fact, is best addressed as multi-objective optimization that allows espousing any one to the exclusion of others. This confronts us with the fact

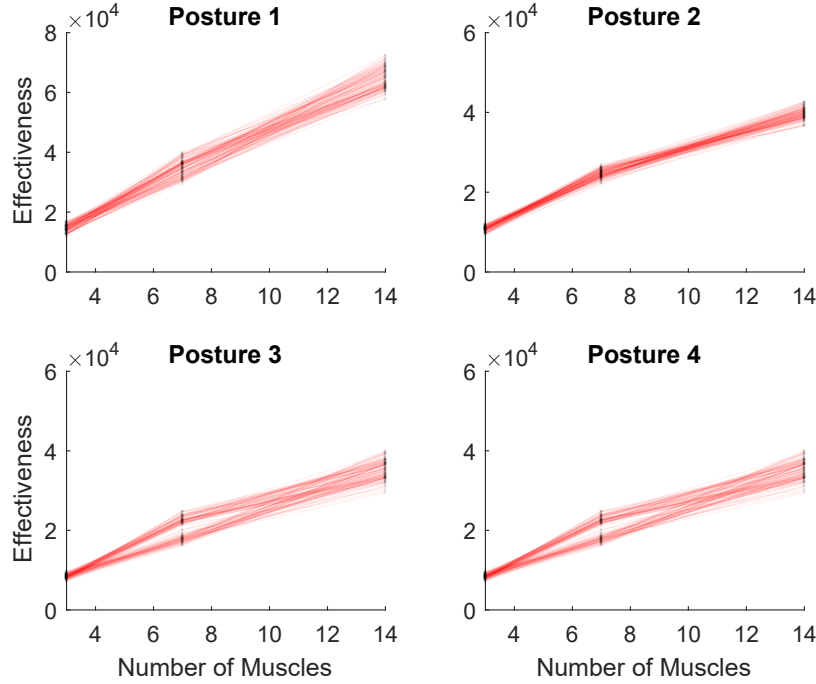


**Fig. 10** Effectiveness plots (Monte Carlo analysis).

that any cost function is, in essence, a reflection of the multiple fitness criteria that may have been achieved, are being pursued, or are even changing in the environment. Thus, a change in environment, goals and life habits, over time, may naturally change the number and/or routing of muscles in a given anthropomorphic system. In addition, although the general patterns between simulations and real systems match, it is important to keep in mind the simplifications that were made, when comparing results from simulations to physiological recordings.

### 3 Does a minority of the variance contain a majority of information?

In this section, we explore the risks of assuming that a low-dimensional approximation suffices to capture the versatility of anthropomorphic systems. We have shown that, although a few Principal Components (PCs) can explain most of the variance in a specific movement or a set of gestures, the remaining variance can in fact contain critical details. This highlights that the reduction of DOF will come at the cost of

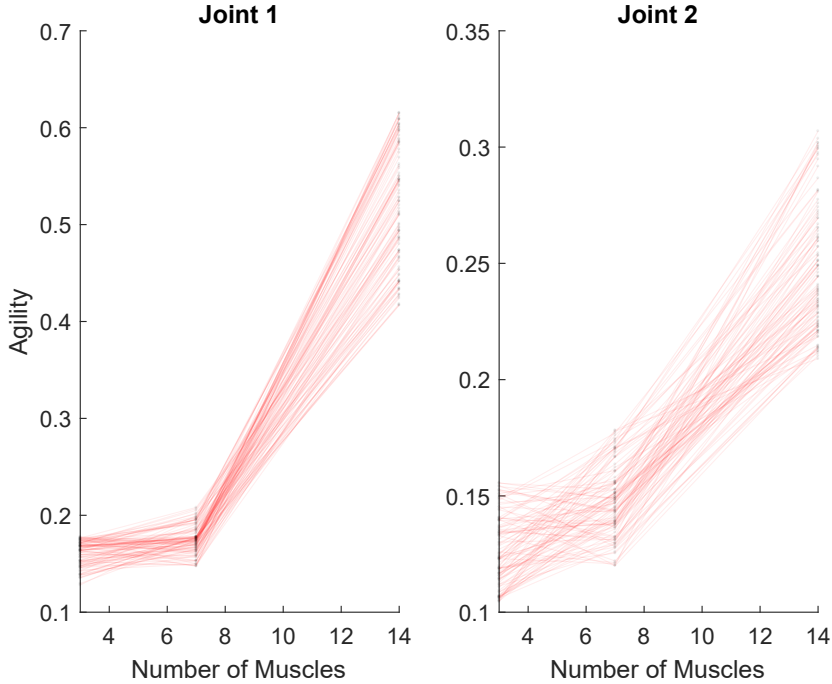


**Fig. 11** Agility plots for each of the two joints (Monte Carlo analysis).

versatility. Therefore, the fact that a few PCs capture a most of variance does not mean that anthropomorphic systems should be low-dimensional.

The problem of face recognition serves as a useful analogy. Human faces all share common features, e.g. we generally have two eyes, two ears; and the general placement of the mouth, nose, eyes and ears follows a specific pattern. However, we can recognize a particular face from among many only due to its small differences compared to the others. Similarly, when talking about hand gestures, postures and functions, the details can become very important to a specific task.

### 3.1 Background

It is known that different sets of motor actions share many commonalities. For example, a linear combination of a small set of basis vectors in a set of movements can explain large amounts of variance for each movement pattern in the set [24]. It is also true for static postures, which means a linear combination of a few basis vectors can explain large amounts of variance in a multi-DOF system; like a human

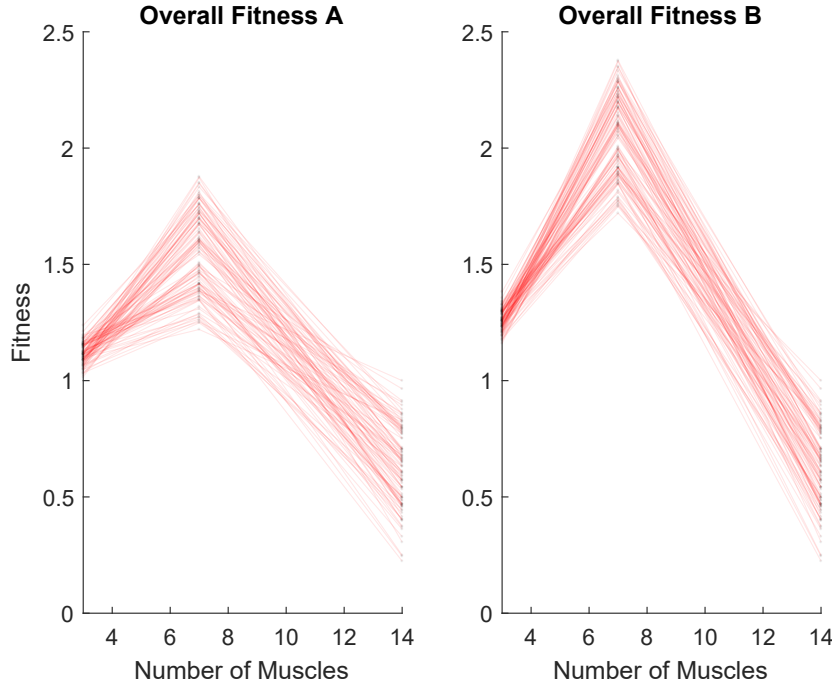


**Fig. 12** Overall Fitness A and B as a function of the number of muscles (Monte Carlo analysis). Note that Phenotypical costs are quadratic (A) or cubic (B) functions that dominate for larger numbers of muscles.

hand [25]. Unfortunately, this is often over-interpreted as a sign that we have more than enough DOF, or as a sign of redundancy in anthropomorphic systems.

We have used principal component analysis (PCA) to extract the principal components (PCs) in a set of hand gestures and shown that although the first few PCs will explain a large amount of variance, all the details that make differentiating between these different movements or postures possible are present in the higher PCs. That is, although higher PCs explain less variance and are generally smaller in amplitude, they are the most important in making postures different from one another. Therefore, these extra DOF are the main contributors to versatility in anthropomorphic systems.

In this section, we further demonstrate this concept with a special focus on hand gestures. We simulate five different hand gestures, comparing and contrasting their representations in the joint angle space (19 joints). We also apply PCA to the joint angle data of these three gestures and demonstrate the effects of utilizing only the first two PCs as compared to all PCs involved.

### 3.2 Method

Grasping gestures of the hand are historically categorized into two main sets: “precision grasp” and “power grasp” [26]. In the former, the thumb and one or more of the remaining fingers will contact the object or apply force in opposition to each other. In the latter, the object will be grasped such that the palm of the hand comes into contact with it [27].

To model our distinct hand gestures, we used MuJoCo, a physics engine which provides accurate simulations for applications including robotics and biomechanics [28]. Five different hand gestures were modeled; two power grasps, two precision grasps, and a non-practical posture which we refer to as the Claw gesture. These five gestures are represented in Fig 13.

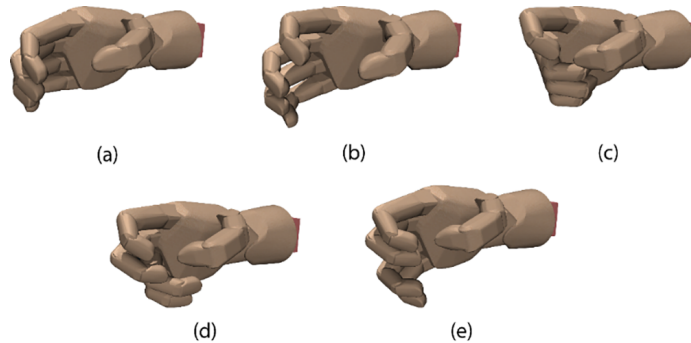


**Fig. 13** 3D model of the five different hand gestures studied in this section. (a) Power grip 1. (b) Power grip 2. (c) Precision grip 1. (d) Precision grip 2. (e) The Claw gesture.

In both power grasps, the fingers opposing the thumb follow similar flexion/extension patterns in their joints. The main difference between power grasps 1 and 2 are the finger abduction values. Index, middle, ring, and pinky fingers have more space between them in power grasp 2 as compared to the power grasp 1. In precision grasp 1, only the index finger opposes the thumb while the other fingers are flexed. In precision grasp 2, the middle finger also opposes the thumb while the other fingers are less flexed. In the Claw gesture, index and ring group together with middle and pinky fingers respectively, and are opposing the thumb.

We extract 19 different joint angles for these three gestures from MuJoCo. These angles are namely Wrist PRO, Wrist UDEV, Wrist FLEX, Thumb ABD, Thumb MCP, Thumb PIP, Thumb DIP, Index ABD, Index MCP, Index PIP, Index DIP, Middle MCP, Middle PIP, Middle DIP, Ring ABD, Ring MCP, Ring PIP, Ring DIP, Pinky ABD, Pinky MCP, Pinky PIP, and Pinky DIP. We then apply PCA (similar to [25]) and compare joint angles of all five gestures before and after applying dimensionality reduction. In the reduced dimension case, we map only the first two PCs back to the joint angle space. We also calculate the Pearson’s correlation coef-

ficient for each pair of gestures in the joint angle space for before and after dimensionality reduction. The Pearson’s correlation coefficient of two different gestures in the joint angle space is defined as follows:

$$\text{Corr}_{i,j} = \frac{\sum_{k=1}^{19} (\text{angle}_{i,k} - \overline{\text{angle}}_i)(\text{angle}_{j,k} - \overline{\text{angle}}_j)}{\sqrt{\sum_{k=1}^{19} (\text{angle}_{i,k} - \overline{\text{angle}}_i)^2} \sqrt{\sum_{k=1}^{19} (\text{angle}_{j,k} - \overline{\text{angle}}_j)^2}} \quad (27)$$

where  $\text{Corr}_{i,j}$  stands for the Pearson’s correlation coefficient between the  $i^{\text{th}}$  and the  $j^{\text{th}}$  gestures and  $\text{angle}_{i,j}$  represents the angle in the  $k^{\text{th}}$  joint of the  $i^{\text{th}}$  posture. Moreover,  $\overline{\text{angle}}_x$  represents the sample average of  $x^{\text{th}}$  gesture and is defined as:

$$\overline{\text{angle}}_i = \frac{1}{19} \sum_{k=1}^{19} \text{angle}_{i,k} \quad (28)$$

In addition, to show the correlations for all five pairs (with and without dimensionality reduction), we created a five by five matrix in which the color of the element on the  $i^{\text{th}}$  row and  $j^{\text{th}}$  column represents the Pearson’s correlation coefficient between the  $i^{\text{th}}$  and the  $j^{\text{th}}$  gesture in the joint angle space. This correlation matrix is defined as follows:

$$C = \begin{bmatrix} \text{Corr}_{1,1} & \cdots & \text{Corr}_{1,j} \\ \vdots & \ddots & \vdots \\ \text{Corr}_{i,1} & \cdots & \text{Corr}_{i,j} \end{bmatrix} \quad (29)$$

### 3.3 Results

The joint angle representation of the hand gestures shown in Fig. 13 are illustrated in Fig. 14a. We apply PCA (as explained in the method section) to filter out the most common component for the five gestures. 91.40% of the variance is explained by the first two PCs. The resulting joint angle space representation for the first two PCs is shown in Fig. 14b.

As can be seen in Fig. 14, with only considering the first two PCs, power grasp 1 and power grasp 2 have grouped together. The same pattern is observed with precision grasp 1 and precision grasp 2. This was within our expectations since by saving the first two PCs, we are ignoring the smaller differences and paying attention to the commonalities.

Figure 15 shows the correlation values for the two cases studied on Fig. 14 colored boxes in the matrix shown in Fig. 15(a) represent the correlation coefficient between the joint angle representation vectors of different gestures. Fig. 15(b) represents the same measure for the case with each gesture only being represented by

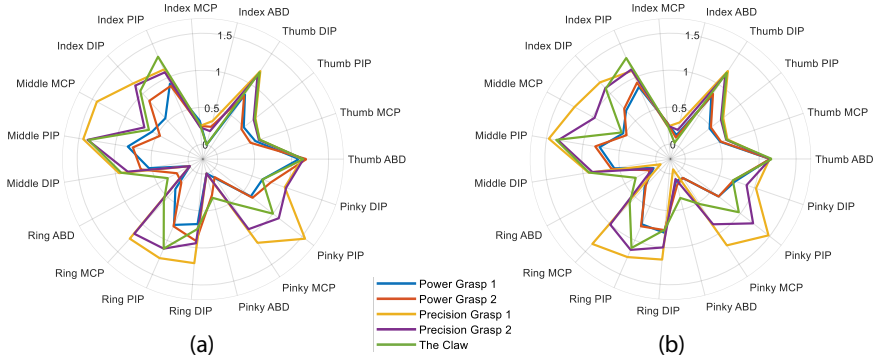


**Fig. 14** Spider plot representations of the 19 joint angles (a) Without dimensionality reduction. (b) With only the first two PCs.

their first two PCs. Comparing Fig. 15(a) and 15(b), we can make three very important observations.

First, in Fig. 15(b), gestures are clustered into three main groups; namely, Power grasp, Precision grasp, and the Claw. These clusters are represented as red squares in Fig. 15(b). This shows that by keeping only the first two PCs, the intra-group correlation values have increased i.e. intra-group dissimilarities have decreased. Furthermore, all group members have lost their distinctions in the reduced dimension space to some extent.

Second, the correlation between gestures in power grasp and gestures in precision grasp groups (inter-class similarity) have become smaller and nearly converged to the same value for any pair of gestures from these two groups. This is illustrated as the dark and light blue lines on the intersections of the power grasp and precision grasp clusters in Fig 15(b). This is significant because in the reduced dimension space, dissimilarity values between any of the power grasp gestures with any of the precision grasp gestures are almost the same. This means that distinguishing different gestures from each other is much more difficult in the reduced dimension space.

Third, the Claw gesture is much more closely correlated to other gestures in the reduced dimensional space. This is mostly observed between the correlation values of the Claw and power grasp 2, and also between the Claw and precision grasp 2. This, again, makes an accurate distinction between the different gestures more challenging. This was observed even though the Claw gesture is a non-practical gesture, which is unlikely to be used in day to day activities.

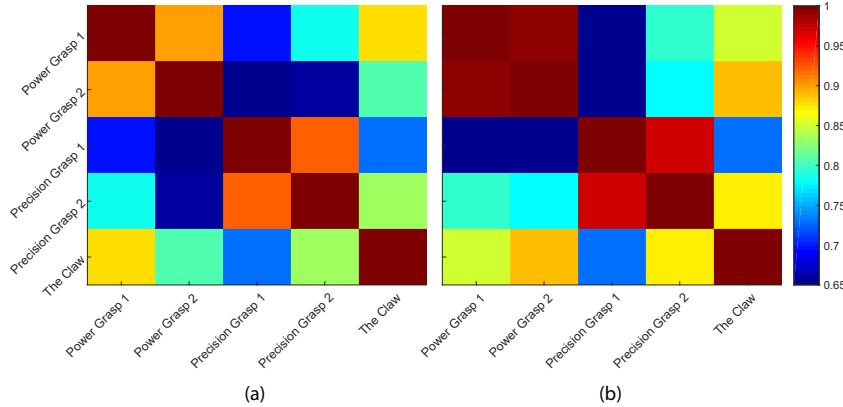


**Fig. 15** The correlation coefficients for each of the gesture pairs. (a) Without dimensionality reduction. (b) With only the first two PCs.

## 4 Chapter conclusions and future work

In this chapter, we took three different approaches to address the question: “Should anthropomorphic systems be redundant?”

In the first section, we presented the classical approach to muscle redundancy for joint torque and endpoint force production in tendon-driven systems. The notion of muscle redundancy holds that there are many ways in which tendon-driven anthropomorphic systems can activate muscles to generate the desired net torques at each joint [17, 18]. However, we underscore that tendon-driven systems are, in fact, *over-determined* from the perspective of *tendon excursions* [1, 6, 14]. That is, the lengths and velocities of all muscles crossing a joint, or set of joints, are determined by the rotations at those joints. From a mechanical perspective, this means that a given limb movement defines a unique set of tendon excursions and velocities. Muscles that shorten during the movement can, in principle, go slack (but then they do not contribute to torque production). However, muscles that lengthen during the movement must do so as specified by the joint rotations. This poses a practical problem in the case where motors are not backdrivable or muscles have stretch reflexes: any muscle that does not lengthen appropriately will disrupt the movement. Therefore, the controller (be it neural or engineered) seeking to produce smooth and accurate movement in a tendon-driven system is not necessarily confronted with a redundant system, as is typically assumed. Rather, it must excite muscles to produce the necessary time history of joint torques *while* allowing muscles to lengthen in the precise way needed. This perspective is not new. Sherrington emphasized the importance of inhibition as a central requirement for the production of movement over 100 years ago [29, 30]. We therefore propose that it is critical for researchers today to pursue a neo-Sherringtonian research direction to understand the robotic and neural control of movement.

The fact that moving smoothly and accurately is neither a redundant, simple, nor a forgiving control problem for tendon-driven systems poses several critical research directions. For example, why does such behavior take years to perfect during typical development in humans (and still not fully available in robot), and why is it so susceptible to developmental and neurological conditions? We propose that the over-determined nature of muscle excursions makes the problem of producing smooth and accurate movements unforgiving to even small errors in development and neurological conditions, which requires further study [1, 6, 14].

In addition, there is emerging evidence that cardinal features of healthy force and movement variability (which are often considered to have cortical origins) can arise naturally as a consequence of the neural control of afferent muscles (i.e., where regulating reflex gains is critical) [31–33]. This opens new research directions to begin to explain, from a purely spinal and peripheral perspective, the clinical presentation of at least some types of tremor in neurological conditions.

The second approach described some aspects of Feasibility Theory, which helps us understand how the anatomy of the plant, and the mechanical constraints that define the task, determine the dimensionality and structure of its feasible activation set (i.e., the family of all feasible commands that can accomplish the task). Such feasible activation sets are well-structured, low-dimensional subspaces embedded in the high-dimensional space of muscle activations. Thus, future research should focus on how the controllers of anthropomorphic systems can explore, identify, exploit, and remember those feasible activation sets. After all, the most any neural or engineered controller can do is explore and exploit the capabilities of the tendon-driven system as a whole [1].

Another important aspect of Feasibility Theory is that the number of independently controllable muscles also determines the number of independent task constraints that tendon-driven systems can satisfy [1, 16]. Thus, adding and having more (appropriately placed) muscles may, in fact, be the critical enabler of ecological (i.e., real-world) function. That is, more muscles enable performing more complex tasks—where complexity is taken to mean the need to meet more task constraints simultaneously. Thus, it is important to investigate how ecological tasks necessitate having more muscles than are apparently necessary when studying “simpler” experimental tasks [2]. This implies that failure to control all muscles independently (as is common in, say, stroke) will reduce functional capabilities because independent muscle control is necessary to meet the multiple requirements of ecological tasks. Thus, “redundant” systems with many muscles (or control DOFs in general) are functionally desirable.

Importantly, these findings also motivate further research on the advantages and disadvantages of muscle synergies (where several muscles are activated in a correlated manner, effectively reducing the number of independent control DOFs). Given that implementing muscle synergies can be an effective way to control robots [34]—and assess limb movement [35]—exploring the relationship between the number of independent control DOFs and functional versatility requires further study [4, 11, 24, 36].

The second section also approached the classical problem of muscle redundancy from the perspective of multi-objective optimization. That is, tackling simultaneous and independent functional goals. As an example, we explored three: maximal endpoint force, maximal joint angular velocities, and the Phenotypical cost of having additional muscles. We showed how an anthropomorphic system can adapt to consider all three goals to arrive at a most desirable number of muscles (yet sub-optimal with respect to individual cost functions). Moreover, this desirable number of muscles is a function of the relative weighing across goals. We find that more muscles allow the limb to be better at multiple goals. Moreover, this study underscored how a change in environment, goals, and life habits may, over time, naturally change the number and/or routing of muscles in a given anthropomorphic system, and vice versa.

The third and last section highlights our final approach to the question: “Should anthropomorphic systems be redundant?” We first showed how, in agreement with [25], more than 90% of the variance in different hand gestures studied here can be explained with only two principal components. However, disregarding the remaining PCs will naturally make it more difficult to distinguish and/or implement each gesture. This example highlights a little-appreciated—in our opinion—consequence in dimensionality reduction: that it will make it very difficult to distinguish similar hand gestures with different functional roles as per well-known grasp taxonomies [37]. For example, a power grasp with the thumb abducted serves to oppose the fingertips. If the thumb is slightly adducted, it can press against the side of the fingers to roll an object with high precision (see Figure 3 in [37]). Thus, although the higher PCs explain ever-decreasing percentages of variance, they nevertheless have important functional consequences. This is in agreement with recent findings in the field of soft robotics. Such studies show how small amounts of passive deformation, provided by non-stiff materials, can significantly increase the functional capabilities, robustness, and versatility of under-actuated hands [4, 38, 39]. Therefore, finding that some PCs that explain relatively little variance does not necessarily mean that the system has unnecessary DOFs or is functionally redundant.

## MATLAB toolbox

All the simulations demonstrated in this chapter were performed using a custom Neuromechanics toolbox written in MATLAB. This toolbox is available at [github.com/marjanin/Neuromechanics-Toolbox](https://github.com/marjanin/Neuromechanics-Toolbox) and at [ValeroLab.org](http://ValeroLab.org).

## Acknowledgements

This study was supported by the National Institute of Arthritis and Musculoskeletal and Skin Diseases of the National Institute of Health (NIH) under award numbers R01 AR-050520 and R01 AR-052345 to FVC, and University of Southern California Graduate Schools Provost Fellowship to AM. The content is solely the respon-

sibility of the authors and does not necessarily represent the official views of the NIH.

We acknowledge Dr. Christopher Laine and Amir Ahmadi for their helpful comments on this manuscript. We thank the University of Southern California for facilities provided during the course BME/BKN 504 and Antara Dandekar and Monica Guerrero for their help with the conceptualization of Section II.

## References

1. F. J. Valero-Cuevas, *Fundamentals of neuromechanics*, vol. 8. Springer, 2015.
2. G. E. Loeb, “Overcomplete musculature or underspecified tasks?,” *Motor control*, vol. 4, no. 1, pp. 81–83, 2000.
3. K. Ogata and Y. Yang, “Modern control engineering,” 1970.
4. O. Brock and F. Valero-Cuevas, “Transferring synergies from neuroscience to robotics comment on hand synergies: Integration of robotics and neuroscience for understanding the control of biological and artificial hands by m. santello et al.,” *Physics of life reviews*, vol. 17, p. 27, 2016.
5. J. Rieffel, F. Valero-Cuevas, and H. Lipson, “Automated discovery and optimization of large irregular tensegrity structures,” *Computers & Structures*, vol. 87, no. 5, pp. 368–379, 2009.
6. D. A. Hagen and F. J. Valero-Cuevas, “Similar movements are associated with drastically different muscle contraction velocities,” *Journal of Biomechanics*, 2017.
7. L. U. Odhner, L. P. Jentoft, M. R. Claffee, N. Corson, Y. Tenzer, R. R. Ma, M. Buehler, R. Kothout, R. D. Howe, and A. M. Dollar, “A compliant, underactuated hand for robust manipulation,” *The International Journal of Robotics Research*, vol. 33, no. 5, pp. 736–752, 2014.
8. Y.-T. Lee, H.-R. Choi, W.-K. Chung, and Y. Youm, “Stiffness control of a coupled tendon-driven robot hand,” *IEEE Control Systems*, vol. 14, no. 5, pp. 10–19, 1994.
9. H. Kobayashi, K. Hyodo, and D. Ogane, “On tendon-driven robotic mechanisms with redundant tendons,” *The International Journal of Robotics Research*, vol. 17, no. 5, pp. 561–571, 1998.
10. J. L. Fu and N. S. Pollard, “On the importance of asymmetries in grasp quality metrics for tendon driven hands,” in *Intelligent Robots and Systems, 2006 IEEE/RSJ International Conference on*, pp. 1068–1075, IEEE, 2006.
11. J. M. Inouye, J. J. Kutch, and F. J. Valero-Cuevas, “A novel synthesis of computational approaches enables optimization of grasp quality of tendon-driven hands,” *IEEE Transactions on Robotics*, vol. 28, no. 4, pp. 958–966, 2012.
12. J. M. Inouye and F. J. Valero-Cuevas, “Anthropomorphic tendon-driven robotic hands can exceed human grasping capabilities following optimization,” *The International Journal of Robotics Research*, vol. 33, no. 5, pp. 694–705, 2014.
13. K. L. Mardula, R. Balasubramanian, and C. H. Allan, “Implanted passive engineering mechanism improves hand function after tendon transfer surgery: a cadaver-based study,” *Hand*, vol. 10, no. 1, pp. 116–122, 2015.
14. F. J. Valero-Cuevas, B. Cohn, H. Yingvason, and E. L. Lawrence, “Exploring the high-dimensional structure of muscle redundancy via subject-specific and generic musculoskeletal models,” *Journal of biomechanics*, vol. 48, no. 11, pp. 2887–2896, 2015.
15. U. Proske and D. Morgan, “Muscle damage from eccentric exercise: mechanism, mechanical signs, adaptation and clinical applications,” *The Journal of physiology*, vol. 537, no. 2, pp. 333–345, 2001.
16. J. M. Inouye and F. J. Valero-Cuevas, “Muscle synergies heavily influence the neural control of arm endpoint stiffness and energy consumption,” *PLoS computational biology*, vol. 12, no. 2, p. e1004737, 2016.

17. R. D. Crowninshield and R. A. Brand, “A physiologically based criterion of muscle force prediction in locomotion,” *Journal of biomechanics*, vol. 14, no. 11, pp. 793–801, 1981.
18. E. Chao and K.-N. An, “Graphical interpretation of the solution to the redundant problem in biomechanics,” *Journal of Biomechanical Engineering*, vol. 100, no. 3, pp. 159–167, 1978.
19. T. Yoshikawa, *Foundations of robotics: analysis and control*. MIT press, 1990.
20. J. Leijnse, “A generic morphological model of the anatomic variability in the m. flexor digitorum profundus, m. flexor pollicis longus and mm. lumbricales complex,” *Cells Tissues Organs*, vol. 160, no. 1, pp. 62–74, 1997.
21. F. E. Zajac, “Muscle and tendon properties models scaling and application to biomechanics and motor,” *Critical reviews in biomedical engineering*, vol. 17, no. 4, pp. 359–411, 1989.
22. V. Chvatal, *Linear programming*. Macmillan, 1983.
23. B. I. Prilutsky, “Muscle coordination: the discussion continues,” *Motor Control*, vol. 4, no. 1, pp. 97–116, 2000.
24. J. J. Kutch and F. J. Valero-Cuevas, “Challenges and new approaches to proving the existence of muscle synergies of neural origin,” *PLoS computational biology*, vol. 8, no. 5, p. e1002434, 2012.
25. M. Santello, M. Flanders, and J. F. Soechting, “Postural hand synergies for tool use,” *Journal of Neuroscience*, vol. 18, no. 23, pp. 10105–10115, 1998.
26. J. R. Napier, “The prehensile movements of the human hand,” *Bone & Joint Journal*, vol. 38, no. 4, pp. 902–913, 1956.
27. R. S. Johansson and K. J. Cole, “Sensory-motor coordination during grasping and manipulative actions,” *Current opinion in neurobiology*, vol. 2, no. 6, pp. 815–823, 1992.
28. E. Todorov, T. Erez, and Y. Tassa, “Mujoco: A physics engine for model-based control,” in *Intelligent Robots and Systems (IROS), 2012 IEEE/RSJ International Conference on*, pp. 5026–5033, IEEE, 2012.
29. C. S. Sherrington, “Reflex inhibition as a factor in the co-ordination of movements and postures,” *Experimental Physiology*, vol. 6, no. 3, pp. 251–310, 1913.
30. C. S. Sherrington, “Inhibition as a coordinative factor,” *Nobelprize.org*, 1932.
31. C. M. Laine, A. Nagamori, and F. J. Valero-Cuevas, “The dynamics of voluntary force production in afferented muscle influence involuntary tremor,” *Frontiers in computational neuroscience*, vol. 10, 2016.
32. K. Jalaleddini, A. Nagamori, C. M. Laine, M. A. Golkar, R. E. Kearney, and F. J. Valero-Cuevas, “Physiological tremor increases when skeletal muscle is shortened: implications for fusimotor control,” *The Journal of Physiology*, 2017.
33. A. Nagamori, C. M. Laine, and F. J. Valero-Cuevas, “Cardinal features of involuntary force variability can arise from the closed-loop control of viscoelastic afferented muscles,” *PLoS Comp Biol*, 2017, in press.
34. M. Santello, M. Bianchi, M. Gabiccini, E. Ricciardi, G. Salvietti, D. Prattichizzo, M. Ernst, A. Moscatelli, H. Jörntell, A. M. Kappers, *et al.*, “Hand synergies: integration of robotics and neuroscience for understanding the control of biological and artificial hands,” *Physics of life reviews*, vol. 17, pp. 1–23, 2016.
35. L. H. Ting and J. L. McKay, “Neuromechanics of muscle synergies for posture and movement,” *Current opinion in neurobiology*, vol. 17, no. 6, pp. 622–628, 2007.
36. F. J. Valero-Cuevas and M. Santello, “On neuromechanical approaches for the study of biological and robotic grasp and manipulation,” *Journal of NeuroEngineering and Rehabilitation*, vol. 14, no. 1, p. 101, 2017.
37. T. Feix, J. Romero, H.-B. Schmidtmayer, A. M. Dollar, and D. Kragic, “The grasp taxonomy of human grasp types,” *IEEE Transactions on Human-Machine Systems*, vol. 46, no. 1, pp. 66–77, 2016.
38. R. Deimel and O. Brock, “A novel type of compliant and underactuated robotic hand for dexterous grasping,” *The International Journal of Robotics Research*, vol. 35, no. 1–3, pp. 161–185, 2016.
39. M. G. Catalano, G. Grioli, E. Farnioli, A. Serio, C. Piazza, and A. Bicchi, “Adaptive synergies for the design and control of the pisa/iit softhand,” *The International Journal of Robotics Research*, vol. 33, no. 5, pp. 768–782, 2014.